Pulsed-Laser Deposited 35 $Bi(Mg_{1/2}Ti_{1/2})O_3$-65 $PbTiO_3$ Thin Films—Part II: Influence of A-Site Deficiency and Thickness Scaling on Electric Properties

Carl Morandi and Susan Trolier-McKinstry, *Fellow, IEEE*

***Abstract*— 35 $Bi(Mg_{1/2}Ti_{1/2})O_3$-65 $PbTiO_3$ (35 BiMT-65 PT) thin films with varying levels of A-site deficiency were investigated as a potential candidate for high-temperature nonvolatile ferroelectric memories. $PbTiO_3$ seed layers utilized to nucleate the perovskite phase in A-site deficient films induced a thickness dependence to the ferroelectric hysteresis and dielectric permittivity. Adjusting for this, the dielectric response of the 35 BiMT-65 PT films is ≈960. The maximum dielectric permittivity was 430 °C at 1 MHz for A-site deficient films. The transition temperature is independent of film thickness to 85 nm. Tan(δ) remains less than 15% at 1 MHz regardless of film thickness and temperature up to 585 °C. High-temperature polarization–electric field hysteresis measurements show charge injection with increasing temperature, while positive-up-negative-down measurements show little temperature dependence of P_r up to temperatures of 200 °C. Poole–Frenkel emission dominated the high field leakage behavior. The refractive index measured by ellipsometry is 2.58 at 633 nm. All samples show significant retention loss. As the stoichiometry improves, retention improves such that >40% of the initial ΔP is retained over ≈280 min.**

***Index Terms*— A-site deficient perovskite, bismuth magnesium titanate–lead titanate, capacitor in series, ellipsometry, Poole–Frenkel emission, retention.**

I. Introduction

FUNCTIONAL ferroelectric thin films have enabled numerous devices including actuators, sensors, transducers, and energy harvesters [1]. Commercially, ferroelectric films are important in ferroelectric random access memory (FeRAM) [2], [3]. Currently, FeRAM is utilized in consumer electronics, medical equipment, and many other applications [4]. To further diversify the application of FeRAM, this paper focuses on material systems with potential to surpass the current limiting use temperature of 85 °C. Many of the bismuth-based $PbTiO_3$ solid solution systems have high Curie temperatures. However, these systems are not widely investigated for nonvolatile memory and, thus, mapping the underlying processing-microstructure-property relationships is essential to identify the most promising compositions.

Manuscript received December 21, 2017; accepted April 3, 2018. Date of publication April 9, 2018; date of current version August 29, 2018. This work was supported by Texas Instruments. *(Corresponding author: Carl Morandi.)*

The authors are with the Department of Materials Science and Engineering, Pennsylvania State University, University Park, PA 16802 USA, and also with the Materials Research Institute, Pennsylvania State University, University Park, PA 16802 USA (e-mail: csm204@psu.edu; set1@psu.edu).

This paper has supplementary downloadable material at http://ieeexplore.ieee.org, provided by the authors.

Digital Object Identifier 10.1109/TUFFC.2018.2825019

$(1 - x)Bi(Mg_{1/2}Ti_{1/2})O_3$-$xPbTiO_3$ (BiMT-PT) films are investigated here. The system exhibits a broad maximum in the Curie temperature between 26 and 35 mol% BiMT predicted to be between 525 °C and 535 °C [5]–[7]. In bulk ceramics, the remanent polarization (P_r) at the morphotropic boundary ($x = 0.36$) is ≈33–38 $\mu C/cm^2$ and the P_r at $x = 0.5$ was shown to be ≈25 μC/cm [2], [5], [8], [9]. The dielectric constant of bulk morphotropic phase boundary (MPB) BiMT-PT ranges ≈1000 [5], [6] and ≈300–950 [5], [6], [9], [10] for tetragonal compositions between 25 °C and 100 °C. Compositions around the MPB retain their properties up to at least 200 °C [8], [11]. In both single crystal and ceramics, thermal depoling is notable at 300 °C [8], [12]. All of these properties suggest that BiMT-PT is a potential candidate to replace PZT as a high-temperature FeRAM material.

Research in BiMT and BiMT-PT thin films has recently increased. MPB BiMT-PT thin films were studied by Zhong *et al.* [13] and Zhang and Ren [14]. 600-nm $(100)_c$ oriented 63 BiMT-37 PT thin films produced by Zhong *et al.* [13] had a dielectric constant, $T_{\max}$, $d_{33,f}$ and P_r of 1060, 415 °C, 90 pm/V and 24 $\mu C/cm^2$, respectively. Tetragonal 20 BiMT-80 PT films have a ε_r of 620 and fatigue resistance up to 10^8 cycles (films doped with 0.5-mol% Mn) [15]. In addition, the polarization–electric (P–E) hysteresis response is reported to be stable to temperatures of at least 125 °C [15]. Metastable epitaxial (111) BiMT films produced by Oikawa *et al.* [16] show little thickness dependence in polarization–electric field response from 50 to 800 nm. Although BiMT-PT films are potentially interesting for high-temperature FeRAM, there is no study that reports essential film properties for the same film composition.

A previous paper focused on the processing-composition-property relationships of 35 $Bi(Mg_{1/2}Ti_{1/2})O_3$-65 $PbTiO_3$ thin films grown utilizing pulsed laser deposition (PLD) [7]. Under a wide range of processing conditions, films were found to be A-site deficient, particularly with Pb deficiency. The Pb deficiency is believed to be a result of preferential adsorption of Bi. With improved film composition, the remanent polarization P_r and maximum polarization $P_{\max}$ increased.

This paper focuses on the effects of A-site deficiency on other electrical properties of 35 BiMT-65 PT thin films. The relationship between composition, high-temperature-electric

0885-3010 © 2018 IEEE. Personal use is permitted, but republication/redistribution requires IEEE permission.
See http://www.ieee.org/publications_standards/publications/rights/index.html for more information.

field leakage, dielectric response, and the thickness dependence of the thin film properties are investigated.

II. Experimental Procedure

The 35 BiMT-65 PT films were deposited on $PbTiO_3/Pt/Ti/SiO_2/Si$ substrates as reported elsewhere [7]. Either undoped or 5-mol% La-doped $PbTiO_3$ seed layers were deposited on the Pt-coated Si substrates using the sol–gel method to facilitate perovskite nucleation. Lead acetate trihydrate, titanium isopropoxide (97%), lanthanum acetate hydrate, 2-methoxyethanol (2-MOE), and acetylacetone (ACAC) (all from Sigma-Aldrich Inc., St. Louis, MO, USA) were used as raw materials. Lead acetate (40-mol% excess) and lanthanum acetate were dissolved in 2-MOE and distilled in a rotary evaporator under Ar gas flow until precipitation. A ≈0.3–0.4-M solution was made by adding titanium isopropoxide and 2-MOE to the precipitated powder. After refluxing for 3 h, the solution was distilled, and ACAC (22.5 vol% for a 0.15-M solution) was added to reach the final solution molarity. The solution was spun on the substrate at 3000 rpm for 45 s, pyrolyzed at 225 °C and 400 °C for 2 min each, and crystallized at 600 °C under oxygen flow for 1 min. The undoped 0.15 M and a doped 0.075-M solution produced a film thickness of 36 and 16 nm, respectively.

Ceramic targets with varying compositions were batched using standard ball milling, calcination, and sintering. Briefly, Pb_3O_4, $4MgCO_3Mg(OH)_2 \bullet 4H_2O$ (40%–43.5% MgO, Alfa Aesar), TiO_2 (cr-el grade, 99.9%, Ishihara Sangyo Kaisha), and Bi_2O_3 (varistor grade, 99.99%, MCP Metal Specialties) were batched in a stoichiometric ratio and balled milled in ethanol for 24 h. After drying at 85 °C, the powder was calcined at 775 °C for 4 h. Varying amounts of Bi_2O_3, PbO (Pb_3O_4 calcined at 700 °C for 1 h), and $MgCO_3$ excesses were added to the stoichiometric batch to compensate for losses during deposition. The powders were vibratory milled for 12 h, dried, pressed into pellets and sintered at 825 °C for 2–4 h. Ignition losses were taken into account prior to batching.

PLD was used to deposit 35 BiMT-65 PT films on the seeded substrates. For deposition, the chamber was pumped down to $\approx 10^{-6}$–10^{-7} Torr. A 90%/10% O_2/O_3 mixed gas was employed as the background atmosphere during deposition, with chamber pressures between 60 and 340 mTorr. A KrF excimer laser (Lambda Physik Compex 102, Fort Lauderdale, FL, USA) with an energy density of $\approx 1.6 \pm 0.1$ J/cm^2 was used. The laser spot size and laser measured energy are ≈11.3 mm^2 and 180 mJ. The laser deposition frequency was 10 Hz for all samples. Sample thickness was varied by changing the deposition time. For all samples, the target to substrate distance was maintained at 6 cm and the substrate temperature was maintained at 700 °C. Substrates were bonded to the heater block using silver paste to insure good thermal contact. These parameters were chosen based on conditions for growing $BiScO_3$-PT and PMN-PT, as well as further optimization [17], [18].

Electrical properties were assessed using lithographically defined Pt top electrodes. The electrodes were deposited in a Lesker CMS-18 sputter tool at an Ar pressure of 2.5 mTorr, and patterned by liftoff. All electrodes were annealed at 600 °C for 1 min in flowing O_2. The thin film ferroelectric properties were studied using a Radiant precision multiferroic tester. Polarization–electric (P–E) data were taken at 1 and 10 kHz. All positive-up-negative-down (PUND) [3] data were acquired with a 1-ms pulse and 1-ms delays between pulses. Room-temperature dielectric responses were measured using a 30-mV oscillation at 1 kHz using an LCR meter (HP 4284A). High-temperature dielectric responses were measured using a 30-mV oscillation from 1 kHz to 1 MHz using an LCR meter (Agilent HP 4980).

Optical properties of 35 BiMT-65 PT were measured using a Woollam variable angle spectroscopic ellipsometer (VASE). Single crystal $SrTiO_3$ substrates (Crystec, Berlin, Germany) were used for the VASE measurements. Films were grown on $SrTiO_3$ utilizing similar conditions as noted above. Further details on the optical property measurement are in the supplemental materials.

High-temperature measurements were performed on a home built hot stage. The hot stage was built with fiberfrax insulation and ceramic bricks to insulate the side of the hot stage. The top was insulated using silicone sandwiched between two fused quartz plates. The samples are electrically insulated from the copper heating block using an AlN ceramic plate. A K-type thermocouple was bonded to the surface near the sample to measure the temperature.

III. Results and Discussion

For high-temperature FeRAM technology, many parameters are critical. The material must be scalable to maintain a low driving voltage and show high-temperature stability, low leakage, and polarization retention. To determine if 35 BMT-65 PT is a feasible choice for FeRAM devices, each of these aspects was analyzed.

A. Thickness Dependence

It was previously reported that the ferroelectric properties of ≈600–700-nm-thick 35 BiMT-65 PT films had P_r values up to 22 μC/cm^2 [7]. However, current embedded FeRAM operates at thicknesses <100 nm in order to keep the driving voltage to a minimum. Thus, any potential candidate material must exhibit robust functional properties at thickness <100 nm. Fig. 1(a) and (b) shows the P–E and PUND data, respectively, of seeded 35 BiMT-65 PT thin films as a function of 35 BiMT-65 PT film thickness. A decrease in the maximum polarization is observed with decreasing thickness. P_r is relatively constant until the film thickness decreases to <200 nm. The PUND measurements in Fig. 1(b) are in agreement with the P–E measurements.

The ferroelectric properties drop with film thickness; however, the seed layer is expected to play a role in the degradation of both dielectric and ferroelectric properties. In order to assess this, the dielectric response of the films was studied as a function of film thickness. The seed layer was treated as a

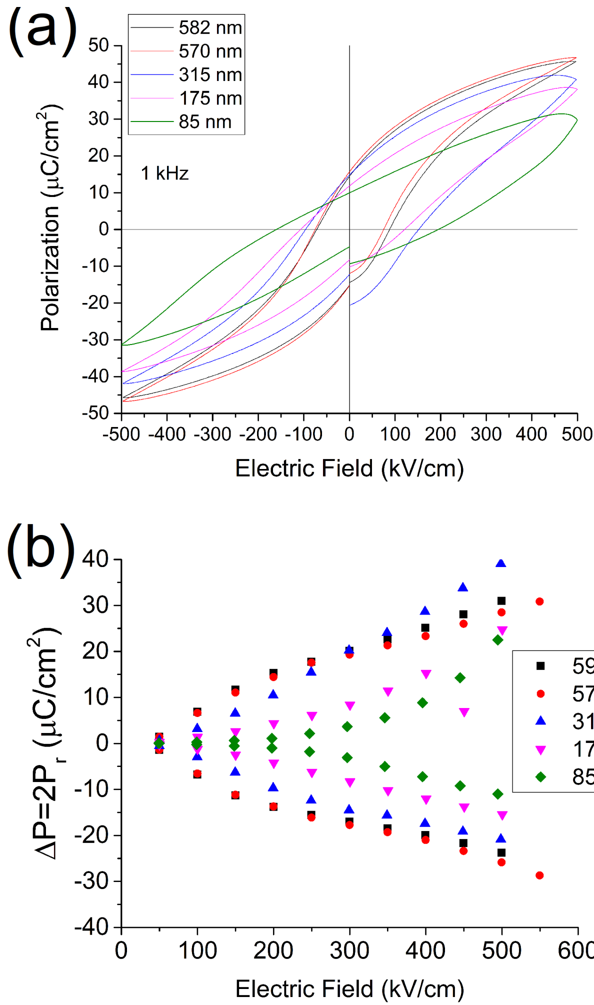

Fig. 1. (a) Ferroelectric P–E and (b) PUND of 35 BiM-65 PT thin films grown on 16-nm 5-mol% La-doped-$PbTiO_3$ seed layer as a function of thickness. The reported thickness is the total film thickness (seed and grown film).

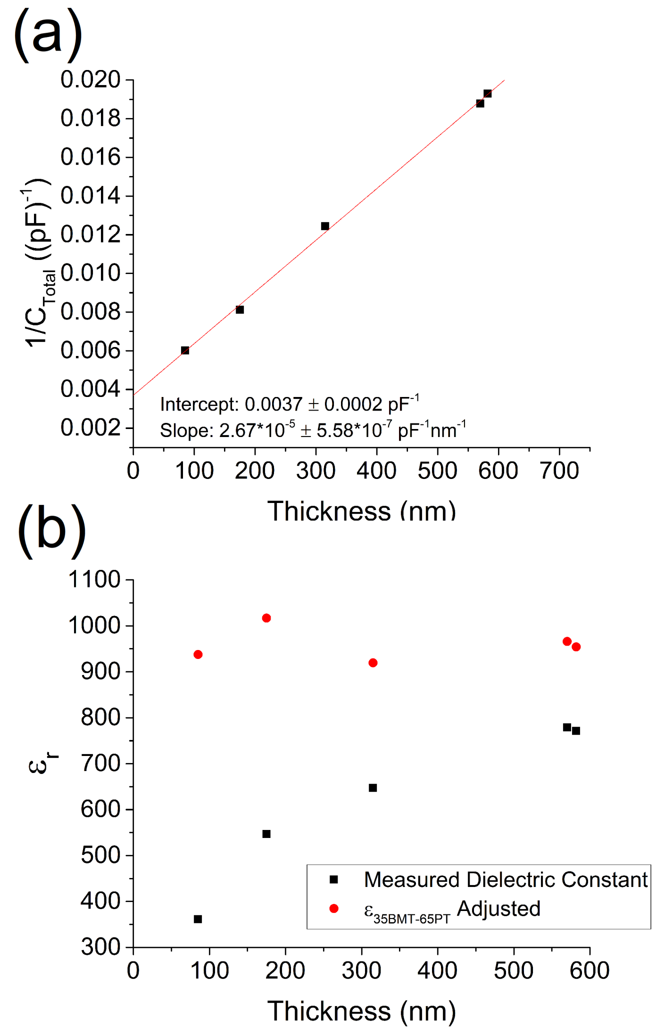

Fig. 2. (a) $1/C_{\text{total}}$ versus thickness plot showing the capacitor in series relationship for seeded 35 BiMT-65 PT thin films. (b) Adjusted versus total film ε_r versus thickness.

capacitor in series

$$\frac{1}{C_{\text{Total}}} = \frac{1}{C_{\text{PbTiO}_3}} + \frac{1}{C_{\text{BiMT-PT}}} \tag{1}$$

where C_{total} is the total capacitance, C_{PbTiO_3} is the capacitance of the seed layer, and $C_{\text{BiMT-PT}}$ is the capacitance of the 35 BiMT-65 PT thin film. Fig. 2(a) shows the capacitance–film thickness relationship, confirming a capacitor in series. The total ε_r for an ≈600-nm film is ≈770; ε_r decreases to ≈360 for an 85-nm film. Fig. 2(b) shows the total ε_r, along with the corrected value for the BiMT-PT layer versus film thickness. The corrected ε_r is ≈960, similar to the ε_r reported by Zhong *et al.* [13] for 63 BiMT-37 PT thin films. The ε_r of the 16-nm $PbTiO_3$ seed is calculated to be 99. The low ε_r seed is expected to contribute to lower net ferroelectric responses in these films.

To further elucidate the relationship between the seed layer and ferroelectric property degradation with thickness, the total switching charge (P*) and nonswitching charge (P^) are plotted as a function of effective electric field and thickness in Fig. 3(a) and (b), respectively. To calculate the effective field, the voltage drop across the seed layer was assumed to be the same ratio to the applied field at all electric fields. The effective field is only an estimation as other charge sources such as domain wall motion, domain switching, and field-dependent leakage may change the ratio. Several phenomena are concluded from these data. First, both positive and negative polarization states show increased leakage with decreasing thickness. The positive P^ polarization charge shows greater amounts of leakage with increasing field and decreasing thickness than the negative polarization charge. Second, P* is constant for all film thicknesses in the negative state. The changes in the positive state are attributed to the increase in P^. Finally, based on the modest change in −P^, the effective coercive field increases for thinner films. This suppression supports the hypothesis that the seed layer contributes to the degradation of the P–E behavior in the BMT-PT with decreasing thickness.

B. Temperature Dependence

The high-temperature behavior was investigated to determine the viability of BiMT-PT for high-temperature FeRAM.

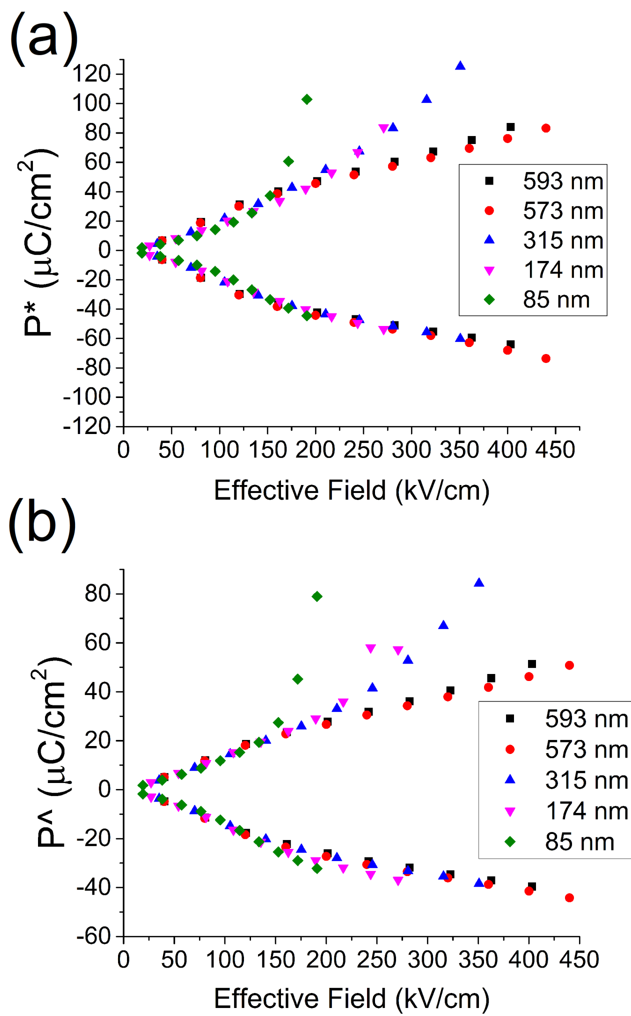

Fig. 3. (a) Switching (P*) and (b) nonswitching (P^) charges versus the effective electric field across the BiMT-PT film of varying thickness. The effective field was calculated, assuming that the percentage voltage drop in the dielectric measurements is constant at all fields and then recalculating the new electric field.

First, the material must have a high T_c to be a viable choice. Fig. 4(a) and (b) shows the ε_r versus temperature behavior of these films. The $T_{\max}$ for an ≈600-nm film is ≈430 °C. The loss tangent [tan(δ)] remains <15% at 1 kHz up to 335 °C and <10% up to 585 °C at 1 MHz. These properties suggest a material that can be utilized in high-temperature applications. It is notable, though that the $T_{\max}$ is significantly below the expected value of ∼530 °C. It is hypothesized that the reduction in $T_{\max}$ is correlated with A-site deficiency, as reported in other perovskite systems. Lee *et al.* [19] observed that as the Ba/Ti ratio in $BaTiO_3$ deviated from 1, the Curie point decreases in the single-phase region of the phase diagram. It is proposed here that a similar mechanism may occur in 35 BiMT-65 PT films. In Bi-based-$PbTiO_3$ solid solutions such as BiMT-PT and BiS-PT, there is not a 1:1 correlation between tetragonality and the phase transition temperature, so it was not possible to use the lattice parameters as an independent indication of the phase transition temperatures. Partial correction of the nonstoichiometry (as reported elsewhere [7]) was achieved using a target with excess in Pb, Bi, and Mg. Fig. 4(c) shows that the $T_{\max}$ increases to 450 °C for this film. It is possible that if the Bi:Pb ratio was fully corrected that $T_{\max}$ would approach the predicted values.

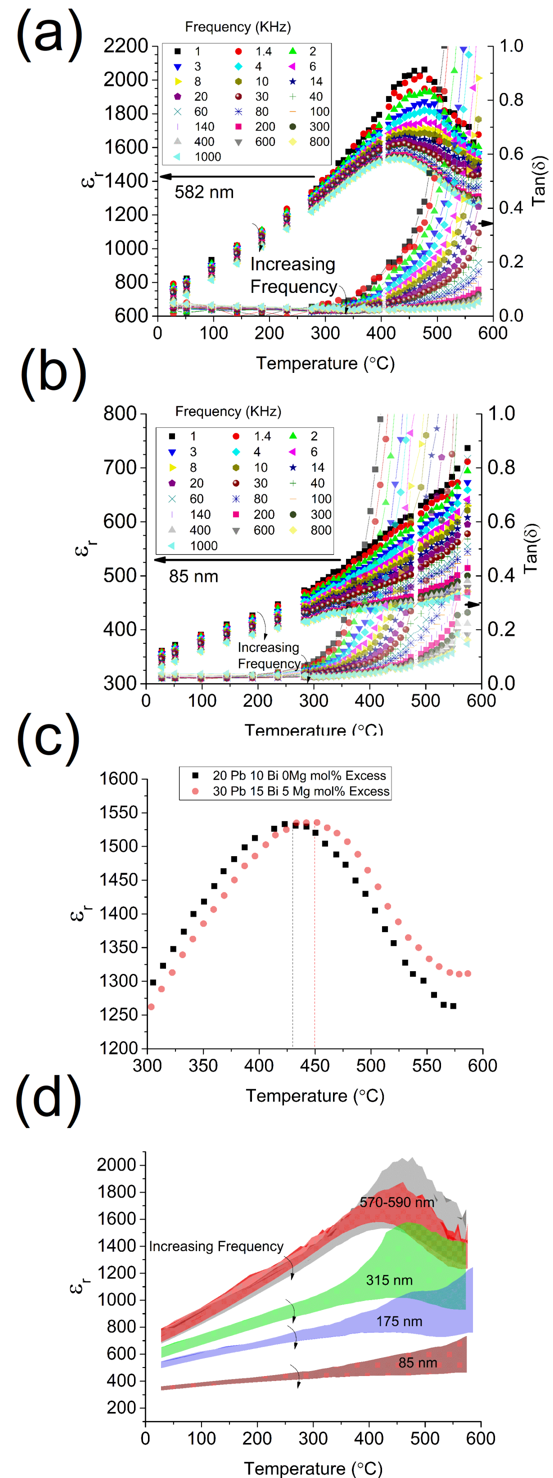

Fig. 4. (a) ε_r versus temperature for a 582-nm-thick film. (b) ε_r versus temperature for a 85-nm-thick film. (c) ε_r versus temperature for films deposited using targets of different compositions. The values refer to the mol% excess of each cation added to the target. Permittivity measurements are at 1 MHz with a 30-mV excitation. Film thicknesses are 582 (squares) and 632 nm (circles). (d) Variety of film thicknesses showing the thickness independence of $T_{\max}$ in 35 BiMT-65 PT thin films.

TABLE I

COMPOSITIONS OF FILMS AS A FUNCTION OF DEPOSITION PRESSURE. THE COMPOSITIONS WERE NORMALIZED SUCH THAT THE TI CONCENTRATION EQUALS THE IDEAL CONCENTRATION. THE OXYGEN CONCENTRATION WAS CALCULATED ASSUMING TYPICAL VALENCES FOR EACH CATION

Pressure	Composition	A/B Site Ratio
60	$(Pb_{0.509}Bi_{0.390}\square_{0.100})(Mg_{0.137}Ti_{0.863})O_{2.958}$	0.90
100	$(Pb_{0.524}Bi_{0.439}\square_{0.036})(Mg_{0.157}Ti_{0.843})O_{3.026}$	0.96
200	$(Pb_{0.517}Bi_{0.439}\square_{0.130})(Mg_{0.160}Ti_{0.840})O_{2.885}$	0.87
340	$(Pb_{0.557}Bi_{0.328}\square_{0.115})(Mg_{0.163}Ti_{0.837})O_{2.886}$	0.88
Ideal	$(Pb_{0.65}Bi_{0.35})(Mg_{0.175}Ti_{0.825})O_3$	1

Moreover, for high-temperature FeRAM, the high T_{max} must be maintained to small film thickness. Fig. 4(d) shows the effect of thickness on the dielectric response (including the seed layer). All films exhibit T_{max} between 430 °C and 440 °C at 1 MHz indicating that the film transition temperature is independent of film thickness to 85 nm. In addition, all films show a loss <15% at 1 MHz up to 585 °C regardless of film thickness. The ε_r at T_{max} becomes less pronounced with decreasing thickness. The suppression of ε_r at T_{max} with decreasing thickness may be attributed to several factors.

1) The presence of the low dielectric permittivity layer in series with the 35 BiMT-65 PT flattens the permittivity peak progressively as film thickness is reduced.
2) The coupling of the domain state with the strain associated with the thermal mismatch between the substrate (Si) and the film [20].

Finally, as T_{max} does not change with thickness, it is anticipated that the polarization state is stable to high temperature regardless of thickness.

As the films show a high T_{max}, the $P–E$ behavior was investigated as a function of temperature. Fig. 5(a) shows the $P–E$ behavior from room temperature to 200 °C for ≈600-nm film. The $P–E$ as a function of thickness shows the same trend as Fig. 1(a) when temperature is increased. Up to 50 °C, no change in $P–E$ is seen. At temperature ≥100 °C, charge injection is seen on one side of the electrodes. The source of the charge injection is discussed later. The negative side of the $P–E$ shows less leakage, and little change up to temperatures of 200 °C. The PUND data shown in Fig. 5(b) for the negative polarization direction confirm the stability to ∼200 °C. While the leakage in the positive direction is problematic for a high-temperature device, the negative polarization state suggests that the problem does not lie with the material, but rather is defect or interface mediated.

C. High-Voltage/Temperature Leakage

While all films have a low dielectric loss tangent (2%–3%) at low field, they exhibit increased leakage with increasing field and temperature. To establish the underlying mechanisms of this behavior, $I–V$ measurements were performed on a series of samples deposited at different deposition pressures on 36-nm $PbTiO_3$ seeds. As discussed in [7], films deposited

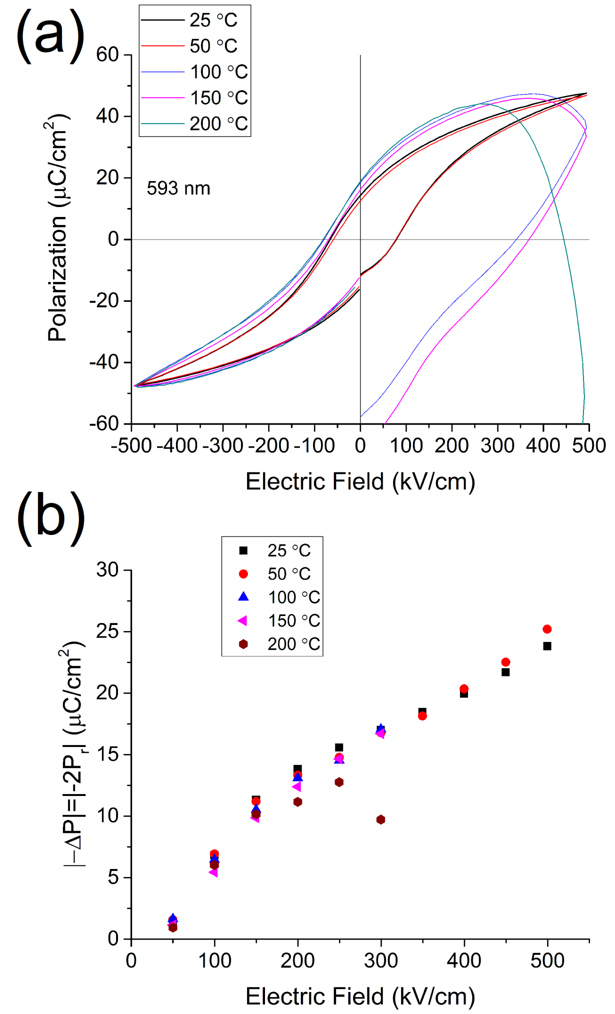

Fig. 5. (a) High-temperature $P–E$ response for a ≈600-nm 35 BiMT-65 PT thin film. (b) Corresponding PUND for the negative polarization state versus temperature showing temperature independence up to 200 °C.

under different deposition pressures exhibit significant changes in film stoichiometry. Fig. 6(a) shows the dc field dependence of the leakage for films deposited at different pressures; the compositions are shown in Table I. The leakage of these films was found to increase with increasing deposition pressure, which correlates with an increasing A-site deficiency in the films.

Two possible sources for the increase in leakage were considered, Schottky emission (2) and Poole–Frenkel emission (3). Linear fits were done from 175 kV to breakdown fields on all samples and a refractive index value was calculated from the estimated permittivity

$$\ln\left(\frac{J}{T^2}\right) = \ln(A) - \frac{q\phi_B}{kT} + \frac{q\sqrt{\frac{qE}{4\pi\varepsilon_r\varepsilon_o}}}{kT} \quad (2)$$

$$\ln\left(\frac{J}{E}\right) = \ln(q\mu N_c) - \frac{q\phi_T}{kT} + \frac{q\sqrt{\frac{qE}{\pi\varepsilon_r\varepsilon_o}}}{kT} \quad (3)$$

where J is the current density, E is the electric field, T is the temperature, A is the Richardson constant, q is the species

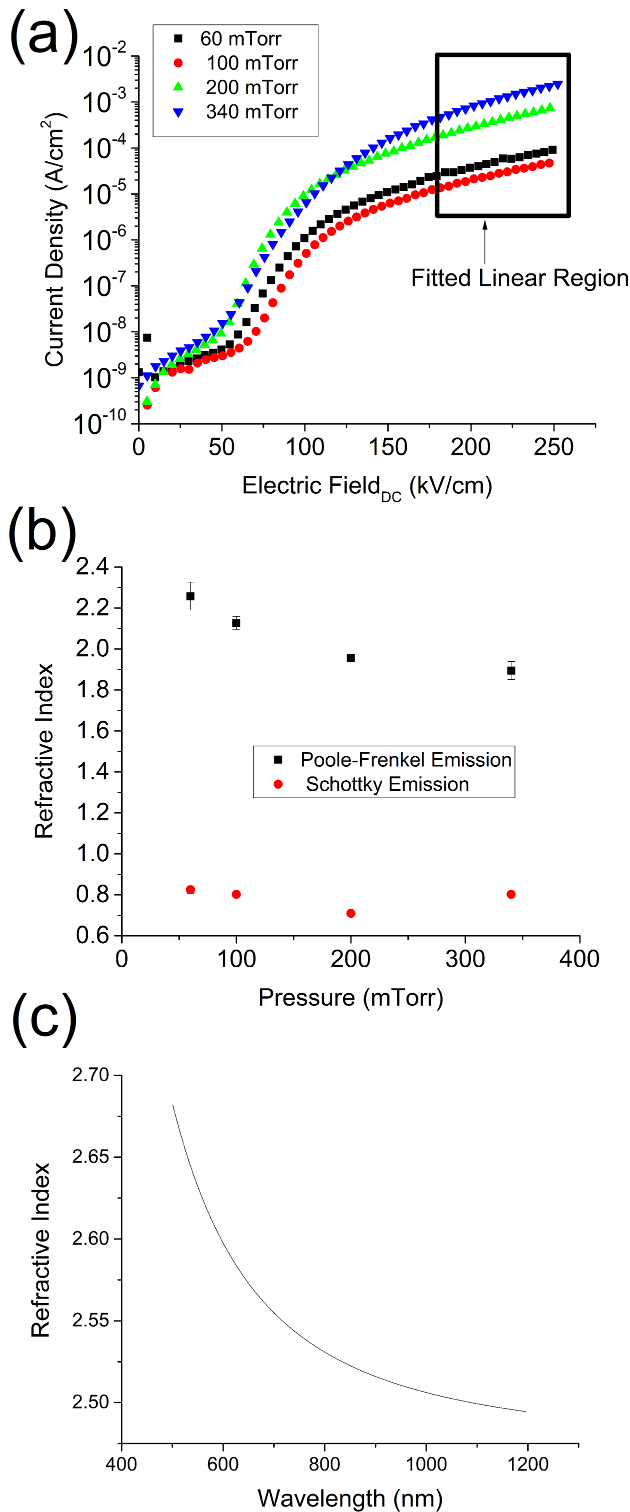

Fig. 6. (a) I–V measurement of 35 BiMT-65 PT thin films deposited under various deposition pressures. (b) Calculated refractive index based on linear fits using the Poole–Frenkel and Schottky models versus deposition pressure. (c) Measured 35 BiMT-65 PT refractive index based on ellipsometry models [31], [32].

charge, φ_B is the barrier height, φ_T is the trap energy level, k is Boltzmann's constant, ε_o is the permittivity of free space, and ε_r is the relative permittivity. See supplemental materials for further details on the permittivity calculation, effect of seed layers, and opposite voltage polarity. The refractive index calculated from the fitting is shown in Fig. 6(b).

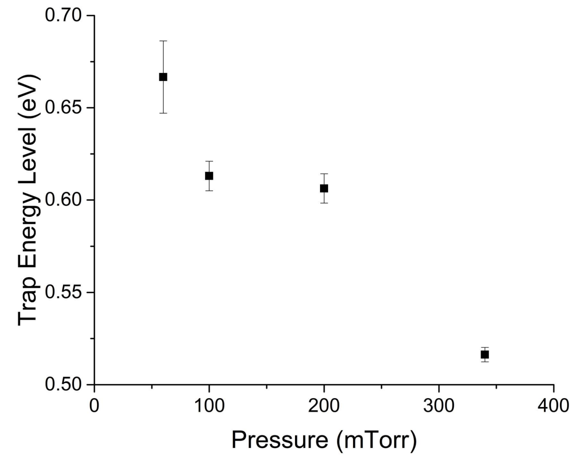

Fig. 7. Estimated trap energy level calculated from I–V versus T measurements.

Fig. 6(c) shows the best-fit refractive index from a spectroscopic ellipsometry measurement of a film grown at 340 mTorr under the same growth conditions using the same target on a $SrTiO_3$ substrate. The substrate and film were modeled using the Sellmeier model

$$n = \left(\varepsilon(\infty) + \frac{A\lambda^2}{\lambda^2 - B^2} - E\lambda^2\right)^{\frac{1}{2}} \quad (4)$$

where A, B, and E are fitting parameters, λ is the wavelength, and $\varepsilon(\infty)$ was set to 1. See supplemental materials for further details on the fitting parameters. At 633 nm, the refractive index is 2.58. Thus, it is apparent from Fig. 6(b) that for all deposition pressures, the Poole–Frenkel model has a more reasonable refractive index than the Schottky model. Furthermore, the refractive index is similar to that of $PbZr_{1-x}Ti_xO_3$ (2.2–2.6), which is reasonable [21]–[32]. This suggests that traps dominate the conduction response; it is hypothesized that the traps are associated with point defects.

Using the refractive index calculated from the I–V measurements, the Poole–Frenkel trap energy level (Fig. 7) was determined to be close to 0.6 eV. The origin of the trap state is unknown, but is reasonably close to the activation energy associated with V_{Pb}' in PZT ceramics ($\approx$0.8 eV). Given the large concentrations of lead vacancies in the 35 BiMT-65 PT films, this seems like a plausible source.

D. Retention

The most basic function of any memory device is the ability to retain information; therefore, as a further assessment of these materials in terms of their potential for FeRAM, their retention properties were evaluated. For this purpose, the same-state retention was explored at room temperature for films. Fig. 8(a) shows the retention of several films deposited using different target compositions. Fig. 8(b) and (c) shows the switching and nonswitching charges for the retention test. Fig. 8(b) shows that there is little systematic change in the

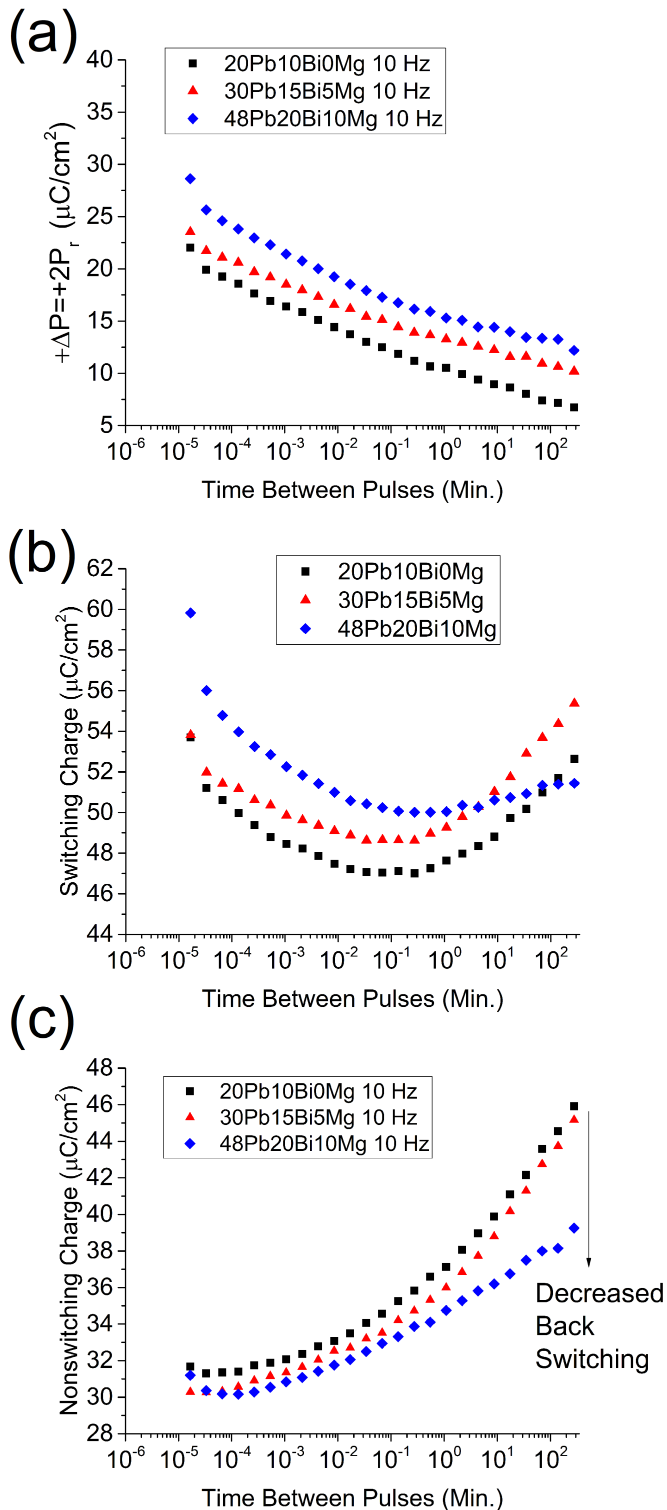

Fig. 8. Room-temperature retention of 580–630-nm 35 BiMT-65 PT thin films as a function of target excess volatile composition. Retention analysis was done with 300 kV/cm and 1-ms pulses. (a) Overall switching response. (b) Switching charge. (c) Nonswitching charge.

switching charge behavior, except that the switching charge increases at small time scales with improved stoichiometry. All films show significant losses in switchable charge over time, which will need to be addressed in future work. It is possible that point defects in the material create internal fields which depole the remanent state. Fig. 8(a) shows that as the Pb, Bi, and Mg concentrations approach stoichiometry (see [7]), the retention increased from ≈30% to >40% of the initial ΔP values after ≈280 min at 0 V. Likewise, Fig. 8(c) shows a systematic decrease in the nonswitching behavior as the film stoichiometry improves. Thus, it is anticipated that with improved film stoichiometry, the same-state retention of 35 BiMT-65 PT films will improve.

IV. Conclusion

Pulsed laser deposited 35 BiMT-65 PT thin films were investigated. The P–E hysteresis and dielectric permittivity were investigated as a function of thickness. With decreasing thickness, the P_r and dielectric permittivity decrease. A capacitor in series model shows that the film thickness-dependent properties may be related to the presence of a low dielectric constant seed layer at the interface. Adjusting for the dielectric permittivity for the seed layer yields a thickness independent dielectric permittivity of ≈960. High-temperature permittivity measurements show a $T_{\max}$ of ≈430 °C and $\tan(\delta) < 15\%$ at 1 MHz up to 585 °C for film thickness between 85 and 600 nm. The high-temperature P–E response show charge injection with increasing temperature. PUND measurements show little change in P_r up to temperatures of 200 °C. I–V measurements show conduction consistent with Poole-Frenkel emission. The retention improves with improved film stoichiometry, suggesting the poor retention is due to defects within the material.

Acknowledgment

The authors would like to thank K. R. Udayakumar, J. Rodriguez, and S. Bhaskar at Texas Instruments, Dallas, TX, USA, for their technical discussions.

References

[1] P. Muralt, R. G. Polcawich, and S. Trolier-McKinstry, "Piezoelectric thin films for sensors, actuators, and energy harvesting," *MRS Bull.*, 35, no. 9, pp. 658–664, Sep. 2009.

[2] J. Rodriguez *et al.*, "Reliability of ferroelectric random access memory embedded within 130 nm CMOS," in *Proc. Reliab. Phys. Symp. (IRPS)*, 2010, pp. 750–758.

[3] J. A. Rodriguez *et al.*, "Reliability properties of low-voltage ferroelectric capacitors and memory arrays," *IEEE Trans. Device Mater. Rel.*, vol. 4, no. 3, pp. 436–449, Sep. 2004.

[4] K. R. Udayakumar *et al.*, "Low-power ferroelectric random access memory embedded in 180 nm analog friendly CMOS technology," in *Proc. 5th IEEE Int. Memory Workshop (IMW)*, May 2013, pp. 128–131.

[5] C. A. Randall, R. Eitel, B. Jones, T. R. Shrout, D. I. Woodward, and I. M. Reaney, "Investigation of a high Tc piezoelectric system: $(1-x)\mathrm{Bi(Mg_{1/2}Ti_{1/2})O_3} - (x)\mathrm{PbTiO_3}$," *J. Appl. Phys.*, vol. 95, no. 7, p. 3633, 2004.

[6] M. R. Suchomel and P. K. Davies, "Predicting the position of the morphotropic phase boundary in high temperature $\mathrm{PbTiO_3}$-$\mathrm{Bi(B'B'')O_3}$ based dielectric ceramics," *J. Appl. Phys.*, vol. 96, no. 8, pp. 4405–4410, 2004.

[7] C. Morandi, J. L. Gray, W. Auker, and S. Trolier-McKinstry, "Pulsed-laser deposited 35 $\mathrm{Bi(Mg_{1/2}Ti_{1/2})O_3}$-65 $\mathrm{PbTiO_3}$ thin films—Part I: Influence of processing on composition, microstructure, and ferroelectric hysteresis," vol. 65, no. 9, pp. 1525–1533, Sep. 2018.

[8] Q. Zhang, Z. Li, F. Li, Z. Xu, and X. Yao, "Temperature dependence of dielectric/piezoelectric properties of (1-x)$\mathrm{Bi(Mg_{1/2}Ti_{1/2})O_3}$− x$\mathrm{PbTiO_3}$ ceramics with an MPB composition," *J. Amer. Ceram. Soc.*, vol. 93, no. 10, pp. 3330–3334, 2010.

[9] S. Sharma and D. A. Hall, "Ferroelectric and antiferroelectric polarisation switching characteristics of $Bi(Mg_{0.5}Ti_{0.5})O_3$–$PbTiO_3$ ceramics," *J. Mater. Sci. Mater. Electron.*, vol. 21, no. 4, pp. 405–409, 2010.

[10] A. Moure, M. Alguero, L. Pardo, E. Ringgaard, and A. F. Pedersen, "Microstructure and temperature dependence of properties of morphotropic phase boundary $Bi(Mg_{1/2}Ti_{1/2})O_3$-$PbTiO_3$ piezoceramics processed by conventional routes," *J. Eur. Ceram. Soc.*, vol. 27, no. 1, pp. 237–245, 2007.

[11] J. Chen, X. Tan, W. Jo, and J. Rödel, "Temperature dependence of piezoelectric properties of high-TC $Bi(Mg_{1/2}Ti_{1/2})O_3$-$PbTiO_3$," *J. Appl. Phys.*, vol. 106, no. 3, p. 34109, 2009.

[12] J. Liu, X. Chen, G. Xu, D. Yang, Y. Tian, and X. Zhu, "Novel high-temperature ferroelectric single crystals $0.38Bi(Mg_{1/2}Ti_{1/2})O_3-0.62PbTiO_3$ with good and temperature-stable piezoelectric properties," *CrystEngComm*, vol. 17, no. 30, pp. 5605–5608, 2015.

[13] C. Zhong, X. Wang, L. Guo, and L. Li, "Characterization of (100)-oriented $0.63BiMg_{1/2}Ti_{1/2}O_3$–$0.37PbTiO_3$ piezoelectric films by a sol–gel process," *Thin Solid Films*, vol. 580, pp. 52–55, Apr. 2015.

[14] L. X. Zhang and X. Ren, "*In situ* observation of reversible domain switching in aged Mn-doped $BaTiO_3$ single crystals," *Phys. Rev. B, Condens. Mater.*, vol. 71, no. 17, pp. 1–8, 2005.

[15] L. Zhang *et al.*, "Temperature-independent ferroelectric property and characterization of high-Tc $0.2Bi(Mg_{1/2}Ti_{1/2})O_3-0.8PbTiO_3$ thin films," *Appl. Phys. Lett.*, vol. 103, no. 8, p. 82902, 2013.

[16] T. Oikawa *et al.*, "Film thickness dependence of ferroelectric properties of (111)-oriented epitaxial $Bi(Mg_{1/2}Ti_{1/2})O_3$ films," *Jpn. J. Appl. Phys.*, vol. 51, no. 9S1, p. 09LA04, 2012.

[17] J. C. Nino and S. Trolier-McKinstry, "Dielectric, ferroelectric, and piezoelectric properties of (001) $BiScO_3$-$PbTiO_3$ epitaxial films near the morphotropic phase boundary," *J. Mater. Res.*, vol. 19, no. 2, pp. 568–572, 2004.

[18] J. Maria, W. Hackenberger, and S. Trolier-McKinstry, "Phase development and electrical property analysis of pulsed laser deposited $Pb(Mg_{1/3}Nb_{2/3})O_3$–$PbTiO_3$ (70/30) epitaxial thin films," *J. Appl. Phys.*, vol. 84, no. 9, pp. 5147–5154, 1998.

[19] S. Lee, C. A. Randall, and Z. K. Liu, "Modified phase diagram for the barium oxide–titanium dioxide system for the ferroelectric barium titanate," *J. Amer. Ceram. Soc.*, vol. 90, no. 8, pp. 2589–2594, 2007.

[20] J. F. Ihlefeld, D. T. Harris, R. Keech, J. L. Jones, J.-P. Maria, and S. Trolier-McKinstry, "Scaling effects in perovskite ferroelectrics: Fundamental limits and process-structure-property relations," *J. Amer. Ceram. Soc.*, vol. 99, no. 8, pp. 2537–2557, 2016.

[21] J. Lappalainen, J. Hiltunen, and V. Lantto, "Characterization of optical properties of nanocrystalline doped PZT thin films," *J. Eur. Ceram. Soc.*, vol. 25, no. 12, pp. 2273–2276, 2005.

[22] A. Deineka, M. Glinchuk, L. Jastrabik, and G. Suchaneck, "Influence of surface and interface on PZT film optical properties," *Phys. Status Solidi*, vol. 175, no. 1, pp. 443–446, 1999.

[23] G. Teowee, J. T. Simpson, T. Zhao, M. Mansuripur, J. M. Boulton, and D. R. Uhlmann, "Electro-optic properties of sol-gel derived PZT and PLZT thin films," *Microelectron. Eng.*, vol. 29, nos. 1–4, pp. 327–330, 1995.

[24] C. H. Peng and S. B. Desu, "Low-temperature metalorganic chemical vapor deposition of perovskite $Pb(Zr_xTi_{1-x})O_3$ thin films," *Appl. Phys. Lett.*, vol. 61, no. 1, pp. 33–36, 1992.

[25] M. P. Moret and M. A. C. Devillers, "Optical properties of $PbTiO_3$, $PbZrxTi_{1-x}O_3$, $PbZrO_3$ films deposited by metalorganic chemical vapor on $SrTiO_3$," *J. Appl. Phys.*, vol. 92, no. 1, pp. 468–474, 2002.

[26] C. H. Peng, J.-F. Chang, and S. B. Desu, "Optical properties of PZT, PLZT, and PNZT thin films," in *Proc. Mat. Res. Soc. Symp.*, 1992, pp. 21–26.

[27] G. Yi, Z. Wu, M. Sayer, G. Vi, and Z. Wu, "Preparation of $Pb(Zr,Ti)O_3$ thin films by sol gel processing: Electrical, optical, and electro-optic properties," *J. Appl. Phys.*, vol. 64, no. 5, pp. 2717–2724, 1988.

[28] C. M. Foster, G.-R. Bai, R. Csencsits, J. Vetrone, and R. Jammy, "Single-Crystal $Pb(Zr_xTi_{1-x})O_3$ thin films prepared by metal-organic chemical vapor deposition: Systematic compositional variation of electronic and optical properties," *J. Appl. Phys.*, vol. 81, no. 5, pp. 2349–2357, 1997.

[29] B. G. Potter, M. B. Sinclair, and D. Dimos, "Electro-optical characterization of $Pb(Zr,Ti)O_3$ thin films by waveguide refractometry," *Appl. Phys. Lett.*, vol. 63, no. 16, pp. 2180–2182, 1993.

[30] A. Deineka, L. Jastrabik, G. Suchaneck, and G. Gerlach, "Ellipsometric investigations of the refractive index depth profile in PZT thin films," *Phys. Status Solidi*, vol. 188, no. 4, pp. 1549–1552, 2001.

[31] S. Trolier-McKinstry, J. Chen, K. Vedam, and R. E. Newnham, "*In situ* annealing studies of sol–gel ferroelectric thin films by spectroscopic ellipsometry," *J. Amer. Ceram. Soc.*, vol. 78, no. 7, pp. 1907–1913, 1995.

[32] S. Trolier-McKinstry, H. Hu, S. B. Krupanidhi, P. Chindaudom, K. Vedam, and R. E. Newnham, "Spectroscopic ellipsometry studies on ion beam sputter deposited Pb $(Zr,Ti)O_3$ films on sapphire and Pt-coated silicon substrates," *Thin Solid Films*, vol. 230, no. 1, pp. 15–27, 1993.

Carl Morandi received the B.S. degree in materials science and engineering from the University of North Texas, Denton, TX, USA, in 2011, and the M.S. degree in materials science and engineering from Pennsylvania State University, University Park, PA, USA, in 2014, where he is currently pursuing the Ph.D. degree with the Materials Science and Engineering Department, with a research focus on high temperature ferroelectric thin film processing for ferroelectric random access memory and piezoelectric devices.

Susan Trolier-McKinstry (M'92–SM'01–F'09) is currently the Steward S. Flaschen professor of ceramic science and engineering, a professor of electrical engineering, and the director of the nanofabrication facility with the Pennsylvania State University, University Park, PA, USA. Her main research interests include thin films for dielectric and piezoelectric applications.

She is a fellow of the American Ceramic Society and the Materials Research Society and an Academician of the World Academy of Ceramics. She currently serves as an Associate Editor for *Applied Physics Letters*. She served as the President of the IEEE Ultrasonics, Ferroelectrics, and Frequency Control Society and Keramos. She was the 2017 President of the Materials Research Society. 21 people that she has advised/co-advised have gone on to take faculty positions around the world.